Journal of Medicinal Chemistry

pubs.acs.org/jmc

Article

Chemoproteomic Profiling of a Carbon-Stabilized Gold(III) Macrocycle Reveals Cellular Engagement with HMOX2

Sailajah Gukathasan,[#] Chibuzor Olelewe,[#] Libby Ratliff, Jong H. Kim, Alyson M. Ackerman, J. Robert McCorkle, Sean Parkin, Gunnar F. Kwakye, Jill M. Kolesar,* and Samuel G. Awuah*

Cite This: https://doi.org/10.1021/acs.jmedchem.4c02952

Read Online

ACCESS | Metrics & More | Article Recommendations | Supporting Information

ABSTRACT: In this work, we discovered a novel organometallic gold(III) macrocycle, **Au-Mac1**, that demonstrates anticancer potency in a panel of triple-negative breast cancer cells (TNBC), and based on this complex, a biotinylated-Au-Mac1 probe was designed for target identification via chemoproteomics, which uncovered the engagement of HMOX2 of the heme-energy metabolism pathway. Using orthogonal chemical biology and molecular biology approaches, including immunoblotting, flow cytometry, and cellular thermal shift assays, it was confirmed that **Au-Mac1** engages HMOX2 in cells. Downstream effects of **Au-Mac1** on the depletion of mitochondrial membrane proteins and bioenergetics point to the potential role of HMOX2 in cancer. Importantly, **Au-Mac1** inhibits in vivo tumor growth of metastatic breast tumor-bearing mice. We believe that this approach is clinically relevant in network-oriented drug discovery. To the best of our knowledge, **Au-Mac1** is the first gold complex that targets HMOX2 to elicit an anticancer effect.

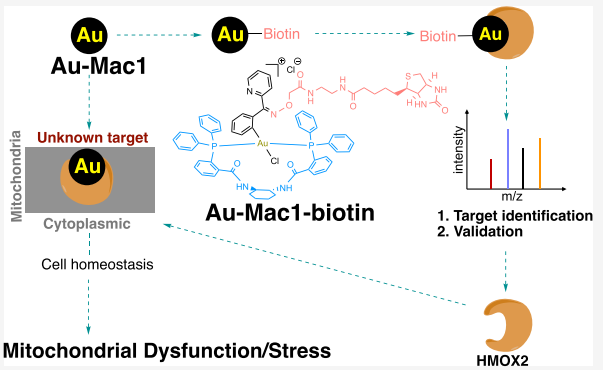

INTRODUCTION

Gold (Au)-derived complexes have gained significant traction as promising therapeutic agents to cure various diseases including rheumatoid arthritis, microbial infections, and cancer.[1,2] Of particular interest are Au(III) complexes with d8 electronic configuration that share isoelectronic and geometric characteristics with Pt(II) complexes, such as cisplatin, a commonly used anticancer chemotherapeutic drug. However, unlike their platinum counterparts, Au(III) complexes often possess unique mechanisms of action due to higher reduction potential (Au(III)/Au(I), 1.41 eV), distinct relativistic effects, and increased polarizability.[3−6] This provides opportunities to address drug resistance and reduce side effects associated with metallodrugs. These alternative mechanisms generally involve interactions with proteins, cellular organelles, and redox pathways, which can trigger apoptosis or other forms of programmed cell death in cancer cells.[7] The discovery and development of novel Au(III) complexes that engage different biological targets to enhance anticancer treatment will be of therapeutic benefit.

The clinical utility of Au(III) complexes has been hampered by challenges related to stability under physiological conditions and the lack of understanding of their biological targets. To address these limitations, we and others have developed Au(III) complexes with strong donor ligands and elucidated mechanisms.[6,8−15] Casini, Hacker, and Meier-Menches and co-workers used chemoproteomic approaches to identify targets of [C^N]-cyclometalated Au(III) dichloride.[16,17] Additionally, macrocycles, which are large cyclic molecules with specific binding sites, have been extensively studied as ligands to stabilize Au(III) ions. Macrocycles form strong chelates with Au(III), shielding the metal center from unwanted chemical transformations while maintaining its bioactivity and fine-tuning physicochemical properties and specific target interactions. The Au(III) macrocycles known are coordination compounds including Au(III) porphyrins, Au(III) corroles, and Au(III) bis(pyrrolide-imine) macrocyclic complexes.[12] Here, we hypothesized that organometallic Au(III) macrocycles will possess optimal stability and a distinct mechanism of action for improved anticancer activity.

The mammalian heme oxygenase family of proteins, HMOX1 and HMOX2 are involved in iron recycling and heme catabolism by catalyzing the stereospecific degradation of heme to biliverdin, carbon monoxide, and free iron.[18] Iron is an important metal in biology with several cellular processes including respiration, ATP production, and ROS removal.[19−21] Thus, iron metabolism is crucial in physiology, but its

Received: December 2, 2024
Revised: February 7, 2025
Accepted: February 10, 2025

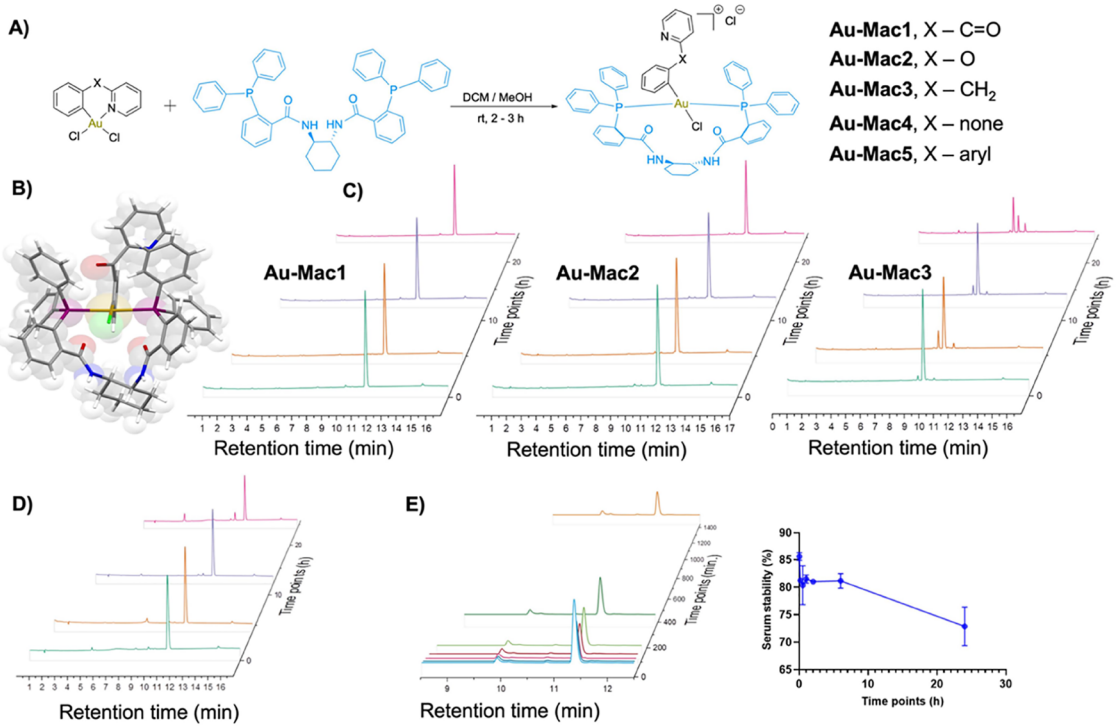

Figure 1. (A) Synthetic scheme for Au-Mac. (B) ORTEP representation of **Au-Mac1** rendered using POV-Ray. Thermal ellipsoids are at the 50% probability level. (C) HPLC plots (mass spectra, Figure S34) of complexes **Au-Mac1, 2** and **3** in RPMI for 24 h. (D) Reaction monitoring of Complex **Au-Mac1** reactivity with GSH (complex 1: GSH = 1:10 or 1:1) for 24 h time using ESI - LC/MS (mass spectra, Figures S36 and S37). (E) Stability of **Au-Mac1** in mouse serum: HPLC chromatogram over 24 h and percentage of complex (%) over 24 h. (n = 2).

disruption leads to related disorders. Whereas HMOX1 is inducible and provides a response to oxidative stress, HMOX2 is constitutively expressed and implicated in physiological signaling, cell proliferation, and tumor initiation.[18,22] Targeting HMOX2 represents a novel strategy in the treatment of cancer. Initial discovery of the antifungal ketoconazole as a non-selective inhibitor of HMOX2 accelerated the search for azole-based modulators of HMOX2.[23] Subsequently, the benzimidazole compound, clemizole (1-(4-chlorobenzyl)-2-(pyrrolidin-1-ylmethyl)-1H-benzimidazole) emerged as a selective inhibitor of HMOX2.[24] Other activators of HMOX2 including menadione, and Vitamin K1, K2, K3 have been reported.[25,26] Recently, a near-infrared probe was identified as targeting HMOX2 with the ability to treat tumor-initiating cells (TICs).[27] High expression levels of HMOX2 are often found in TICs, which are resistant to anticancer therapies and are associated with tumor metastasis and relapse. The persistence of TICs in tumors presents a significant challenge in oncology, making HMOX2 a relevant target for directed therapies. Despite these discoveries, agents targeting HMOX2 are not in clinical development, and the mechanism of small molecule modulation of HMOX2 in the context of a disease is not fully understood.

Effective cancer therapies in the clinic cave to drug resistance and tumor relapse presenting enormous challenges to patient care.[28] An example is breast cancer, which is the second leading cause of cancer mortality in women and is estimated to record ~300,000 new cases in 2023.[29] Protein targets in the context of homeostasis and mitochondrial metabolism that can serve as nodes of multiple signaling networks in each disease indication will likely overcome current oncology challenges associated with breast cancer, particularly the aggressive triple-negative breast cancer (TNBC) and promote precision cancer medicine.[30,31] Therefore, identifying targets with metabolic and homeostatic implications will be ideal and is an unmet need. Recent studies have implicated HMOX2 in the regulation of mitochondria processes[32,33] and targeting human HMOX2 can treat tumor-initiating cells with stem-like character.[27]

In this work, we aimed at elucidating the molecular basis for the disruption of cellular-mitochondrial homeostasis by a new organometallic gold(III) macrocycle using an unbiased chemoproteomic approach. A series of macrocyclic gold(III) complexes with potent anticancer potential demonstrating IC_{50} values in the submicromolar range were evaluated. The complexes can induce mitochondrial dysfunction in cancer cells and antitumor activity in a TNBC mouse model. Using a biotinylated-**AuMac1**, we showed that **Au-Mac1** engages HMOX2, which is an emerging target in cancer. Consequently, **Au-Mac1** depletes mitochondrial fusion proteins, OPA 1 and MFN1 in cancer cells, promotes ROS production, and depolarizes mitochondrial membrane potential. To the best of our knowledge, this is the first report of a gold complex that engages HMOX2 using a rigorous chemical biology approach. We believe this strategy presents a transformative paradigm to the design of homeostatic remodeling perturbants that promote tumor apoptosis.

RESULTS AND DISCUSSION

Synthesis and Solution Stability of AuMacs. Using a green C−H activation protocol in water, cyclometalated (C^N) gold(III) complexes were synthesized from commercially available 2-benzoylpyridine, 2-phenoxypyridine, 2-benzylpyridine, 2-phenylpyridine, and benzo[h]quinoline ligands incorporated with $HAuCl_4{\cdot}3H_2O$. Subsequent associa-

https://doi.org/10.1021/acs.jmedchem.4c02952
J. Med. Chem. XXXX, XXX, XXX−XXX

Table 1. Summary of IC_{50} Values Obtained from MTT Assays in a Panel of Aggressive TNBC Cancer Cell Lines, 72 h Post-treatment

	IC_{50} (μM)				
complexes	MDA-MB-231	MDA-MB-468	MDA-MB-436	SUM159	Hs578T
Au-Mac1	0.56 ± 0.06	0.64 ± 0.27	0.63 ± 0.12	0.61 ± 0.24	0.49 ± 0.12
Au-Mac2	0.43 ± 0.08	0.34 ± 0.22	0.10 ± 0.01	0.40 ± 0.28	0.42 ± 0.15
Au-Mac3	1.15 ± 0.05	2.64 ± 0.18	2.05 ± 0.04	1.80 ± 0.18	1.57 ± 0.13
Au-Mac4	2.26 ± 0.21	1.07 ± 0.19	2.04 ± 0.21	3.82 ± 0.12	4.52 ± 0.41
Au-Mac5	1.97 ± 0.18	1.53 ± 0.11	6.06 ± 0.20	8.33 ± 0.42	6.88 ± 0.45
Auranofin	0.62 ± 0.01	1.92 ± 0.20			
Cisplatin	34.56 ± 0.78	4.72 ± 0.18			
Ligand	≥100	≥100	≥100	≥100	≥100

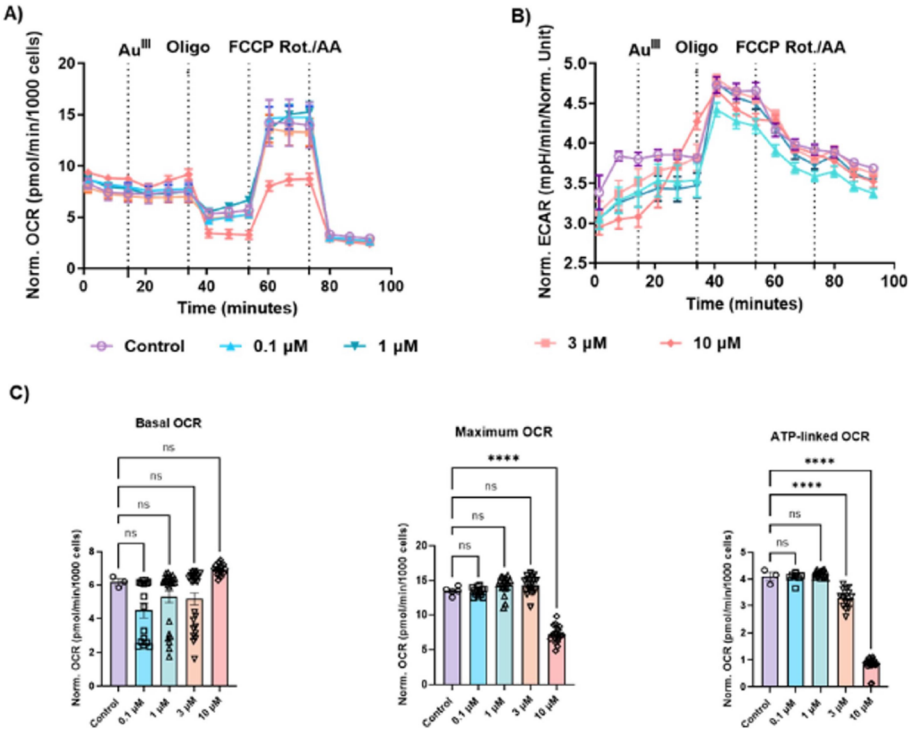

Figure 2. (A) Seahorse bioenergetic stress test of **Au-Mac1** in MDA-MB-468, normalization of the OCR was done per 1000 cells. Data are plotted as the mean ± SEM, $n = 4$ (B) Normalized ECAR data extrapolated from Seahorse metabolism analysis. (C) Bar graphs showing Basal OCR, maximum OCR and ATP-linked OCR readings extrapolated from Seahorse metabolism analysis, Data are plotted as the mean ± SEM ($n = 4$). Data were analyzed by two-way ANOVA ($*p < 0.05$, $**p < 0.01$, $***p < 0.001$, $****p < 0.0001$. n.s. = not significant).

tive ligand substitution with the chiral (R,R)-DACH phenyl Trost ligand resulted in Au-Mac complexes in >80% yield, affording a novel platform for organometallic macrocyclic Au(III) complexes (Figure 1A). X-ray single crystals grown from slow diethyl ether diffusion into saturated chloroform solutions of **Au-Mac1** and **Au-Mac2** support the macrocyclic structure (Figure 1B). All the complexes were characterized by using ^{1}H NMR, ^{13}C NMR, ^{31}P NMR, and low-resolution mass spectrometry (LC/MS), and purity was confirmed by HPLC (>95%) and elemental analysis (Figures S3−S33). A critical bottleneck in metallodrug discovery is the ill-characterized speciation of metal complexes in biological matrices. The solution chemistry and serum stability of **Au-Mac1** were probed via LC-MS (Figures 1C−E, S34−S41). In RPMI media, **Au-Mac1** is unaltered (Figure S34), and in an equimolar reaction of **Au-Mac1** and *L*-glutathione, a dominant biological reductant, **Au-Mac1** remained intact over 24 h (Figure S36). To characterize potential Au-Mac1 intermediates, 1:10 or 1:1000 **Au-Mac1** and L-GSH led to predominantly **Au-Mac1** [m/z 1104.24] and <5% formation of a reduced Au(I) bisphosphine [m/z 887.20] and concomitant *S*-arylated aryl-pyridine motif [m/z 489.14] (Figure S37). In mouse serum, ∼75% of intact **Au-Mac1** is detected over a 24 h period, indicating significant stability of **Au-Mac1** in the relevant biological context.

Anticancer Activity of AuMacs. Several organogold(I/III) complexes induce apoptosis or autophagy in cancer cells via ER stress, mitochondrial dysfunction, and perturb redox homeostasis.[7−9,34−37] Au-Mac model recapitulated similar characteristics in cancer cells. Low inhibitory concentrations (IC_{50}, half-maximal inhibitory concentrations), Table 1) were observed in multiple triple negative breast cancer (TNBC) types including MDA-MB-231 (human breast cancer), MDA-MB-468 (human breast cancer), MDA-MB-436 (human breast cancer), SUM159 (human breast cancer), and Hs578T (human breast cancer) 72 h post **Au-Mac1** treatment using 3-(4,5-dimethylthiazol-2-yl)-2,5-diphenyltetrazolium bromide (MTT) assays (Figure S42). **Au-Mac1** and **Au-Mac2**

https://doi.org/10.1021/acs.jmedchem.4c02952
J. Med. Chem. XXXX, XXX, XXX−XXX

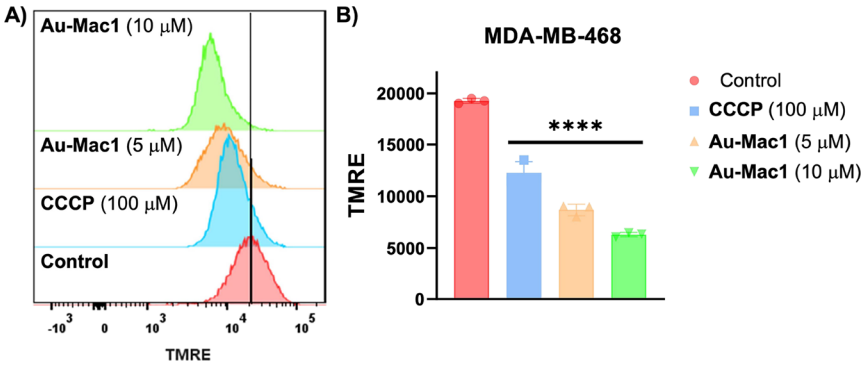

Figure 3. (A) Flow cytometry of tetramethylrhodamine, ethyl ester (TMRE) mitochondrial membrane potential assay analyzing **Au-Mac1** in MDA-MB-468 cells. (B) Bar chart of the effect of **Au-Mac1** on MMP extrapolated from the TMRE dye assay using flow cytometry. Data were analyzed by two-way ANOVA (****$p < 0.0001$.).

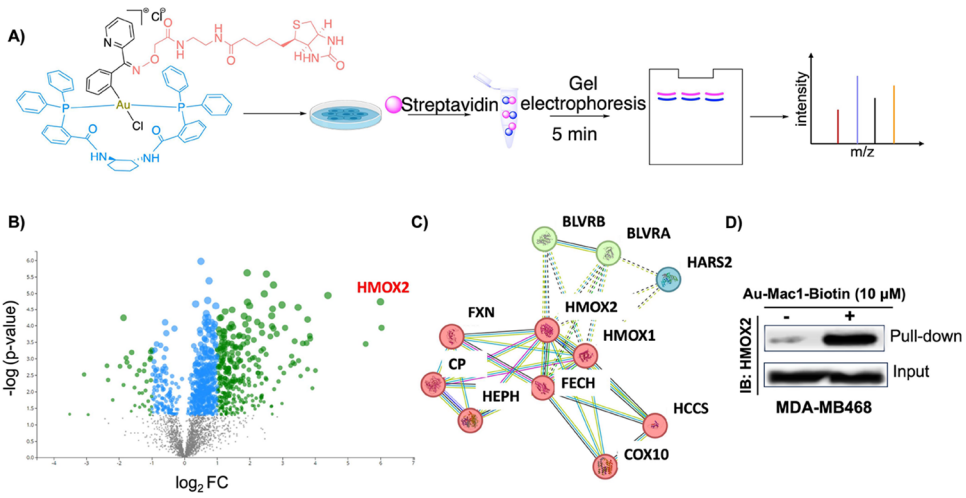

Figure 4. Protein Target Profiling of **Au-Mac1**. (A) Workflow of target protein identification using biotinylated **Au-Mac1** followed by streptavidin capture and LC-MS/MS. (B) Volcano plot displaying differentially expressed proteins. (C) STRING analysis of protein association network related to HMOX2. (D) Immunoblotting of pull-down validation of HMOX2 as the target of **Au-Mac1**-biotin. The input blot is indicative of the amount of HMOX2 in the lysates.

demonstrated superior anticancer activity across the TNBC cells screened. Although **Au-Mac2** was more potent. The synthetic accessibility of a probe compound by functionalizing the keto group of **Au-Mac1** made it a practical option to use for the downstream mechanism of action studies.

AuMac1 Induces Mitochondrial Dysfunction. Since **Au-Mac1** is a lipophilic cation and exhibited potent anticancer activity in a broad panel of aggressive cancer cells, we postulated that the anticancer mechanism of **Au-Mac1** was via mitochondrial pathways. Evidence for disrupted cellular energy homeostasis was confirmed via a MitoStress test by Seahorse XF96. **Au-Mac1** impacted the bioenergetics of TNBCs, MDA-MB-468, or MDA-MB-231 cell lines in a concentration-dependent manner, following pneumatic injection of **Au-Mac1** (Figure 2A, B). For MDA-MB-468, extrapolated basal oxygen consumption rate (OCR) was decreased by 30% compared to control, and maximum OCR was decreased by 50% at 10 μM **Au-Mac1** compared to control. Importantly, ATP-linked respiration, which is a predictor of energy production, was decreased by 75%, and spare respiratory capacity was significantly impacted at 10 μM (Figure 2C). Similarly, in MDA-MB-231 cells, bioenergetic parameters, including basal respiration, maximal respiration, ATP-linked respiration, and spare respiratory capacity, were inhibited by **Au-Mac1** in a concentration-dependent manner (Figure S54). Taken together, **Au-Mac1** induces significant mitochondrial stress.

Further, we evaluated the functional consequence of **Au-Mac1** on mitochondrial membrane polarization by tetramethylrhodamine, ethyl ester (TMRE) assay. TMRE uptake is directly related to $\Delta\Psi_m$ and serves as a reliable indicator of mitochondrial health and function via sequestration by active mitochondria. Additionally, it has fast accumulation, low cytotoxicity, and high sensitivity. Significant mitochondrial membrane depolarization (MMP) arose from fluorescence-assisted cell sorting (FACS) experiments in MDA-MB-468 cells treated with 5 or 10 μM of **Au-Mac1** or 100 μM CCCP along with TMRE MMP marker (Figure 3). We found a dose-dependent decrease in fluorescence signals for **Au-Mac1** treated cells compared to those of CCCP-treated and untreated controls, indicative of strong mitochondrial membrane depolarization by **Au-Mac1**. These studies prompted a detailed study into the plausible molecular target and mechanism of action of **Au-Mac1**. Thus, we hypothesized that a biotinylated probe of Au-Mac1 would facilitate target identification in the context of cancer.

Development of a Biotinylated-AuMac1 Probe. Following the identification of **Au-Mac1** as an inducer of mitochondrial dysfunction, we sought to elucidate its targets by

https://doi.org/10.1021/acs.jmedchem.4c02952
J. Med. Chem. XXXX, XXX, XXX−XXX

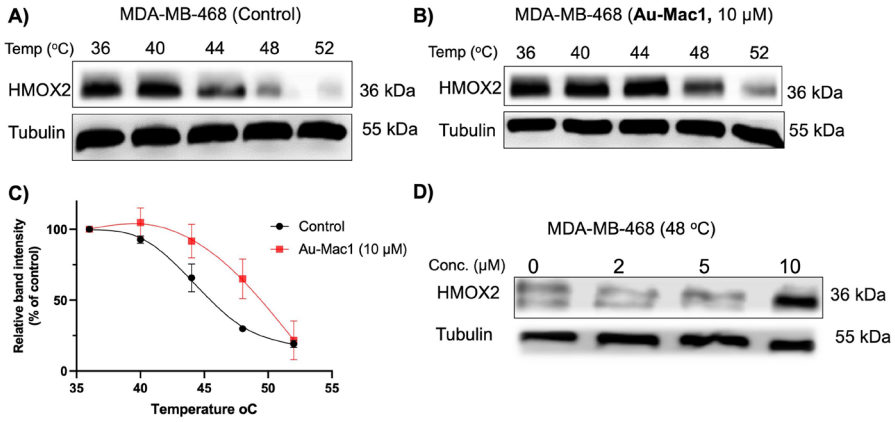

Figure 5. Cellular thermal-shift assay (CETSA) (A) Western blot image of CETSA of HMOX2 at the indicated temperatures. (B) Stabilization of HMOX2 after incubating cells with **Au-Mac1**. (C) CETSA curve showing **Au-Mac1** stabilization of HMOX2. (D) Concentration dependent stabilization of HMOX2 by **Au-Mac1**.

developing a chemical biology probe for a deeper understanding of its mechanism. In this regard, biotin was introduced onto the oxime-functionalized cyclometalated Au(III) dichloride precursor via a peptide linkage. After this, chelation with phosphine donor ligands was performed and purified via flash chromatography to obtain the cationic **Au-Mac1**-biotin probe which was fully characterized by NMR spectroscopy and LC-MS (Scheme S1 and Figures S25−S33).

Chemoproteomic Profiling. To identify the molecular target of **Au-Mac1**, live MDA-MB-468 cells were treated with **Au-Mac1**-biotin at 10 μM for 2 h. The treated cells were lysed, and the lysates were incubated with streptavidin magnetic beads to pull down the biotinylated proteins. The enriched proteins with streptavidin beads from both treated or untreated cells were loaded onto SDS-PAGE and run for 5 min. The gel bands were cut and prepared for tryptic digestion and LC-MS/MS analysis of the enriched peptides to profile the targets (Figure 4A). Proteins not found in the control group while showing a high abundance in the probe treatment group were identified as possible targets. The volcano plot showed HMOX2 as the statistically significant highly ranked differentially expressed protein (Figure 4B).

Additional insight into the protein pathway interactome associated with identified HMOX2 using STRING analysis, a web-based platform for dissecting protein interaction, showed heme metabolism and mitochondrial localization (Figure 4C). Particularly, proteins clustered within the heme metabolic process included BLVRA, BLVRA, and HMOX1. Related mitochondrial proteins involved in iron processing were identified as ferrochelatase, FECH, and cytochrome c oxidase 10 (COX) assembly protein, which catalyzes the farnesylation of the C2 vinyl group of heme, resulting in the transformation of protoheme (heme B) to heme O.[38] It is becoming increasingly clear that perturbing cellular homeostasis has wide metabolic implications leading to effective therapies.[39] Examination of enriched proteins via pull-down studies showed HMOX2 abundance using HMOX2-specific antibodies in an immunoblotting assay, as depicted in Figure 4D.

Validation of HMOX2 Target Engagement by Au-Mac1. Intracellular protein target engagement to verify the interaction of **Au-Mac1** with HMOX2 in MDA-MB-468 cells was performed by a cellular thermal shift assay (CETSA). Based on the phenomenon that ligand-protein binding affects protein stability, Nordlund's group developed CETSA to directly monitor target engagement inside cells.[40] Thermally induced unfolding experiments provide distinct melting curves for a protein, and these melting curves typically shift to a higher temperature when a ligand binds to and stabilizes the target protein.[41] Using CETSA to examine whether **Au-Mac1** binds to endogenous HMOX2, MDA-MB-468 cells treated with or without **Au-Mac1** (10 μM) for 2 h were collected, followed by heating at 36, 40, 44, 48, and 52 °C to denature and precipitate HMOX2 protein, cell lysis, removal of cell debris and aggregates by centrifugation, and finally detection of remaining thermostable HMOX2 protein by Western blot. The HMOX2 aggregation temperatures without **Au-Mac1** were determined to be 44−52 °C but shifted to 48−52 °C after treatment with **Au-Mac1**(Figure 5A−C). Further confirmation by the isothermal dose response CETSA supported the intracellular engagement of HMOX2 by Au-Mac1 as higher concentrations at 10 μM stabilized the protein at the melting temperature of 48 °C (Figure 5D). Overall, we utilized a chemical biology approach to identify and validate a novel Au(III) target.

HMOX2 modulation can influence oxidative stress and mitochondrial membrane depolarization, which promotes the degradation of mitochondrial membrane proteins such as OPA1 and MFN 1&2 via mitophagy.[42] Au agents that rapidly and irreversibly degrade fusion proteins present opportunities to uncover new mechanisms and generate tool compounds and therapeutics for disease. Biochemical hallmarks that characterize fusion protein degradation include: (i) depletion of mitochondrial inner membrane fusion proteins, (ii) autophagy/mitophagy activation, and (iii) modulation of cellular energy homeostasis.[43] Orchestration of these factors in concert suggests mitochondrial dynamics fusion protein degradation in cells. Protein expression of the transmembrane GTPases OPA1 and MFN1, a mitofusin that regulates mitochondrial dynamics and cellular homeostasis was assessed via immunoblotting and found a robust depletion of both proteins in MDA-MB-468 cells by 6−24 h following 1 μM treatment (Figure 6A, B). OPA1 is a fusion protein within the inner mitochondrial membrane, which has been implicated in several cancer mechanisms including cell proliferation, cytochrome C release, and angiogenesis.[44] Furthermore, since disruption of mitochondrial dynamics can lead to cell death,[45] we hypothesized that **Au-Mac1** can induce both mitophagy/autophagy and apoptosis in TNBC. To test this hypothesis, we used

https://doi.org/10.1021/acs.jmedchem.4c02952
J. Med. Chem. XXXX, XXX, XXX−XXX

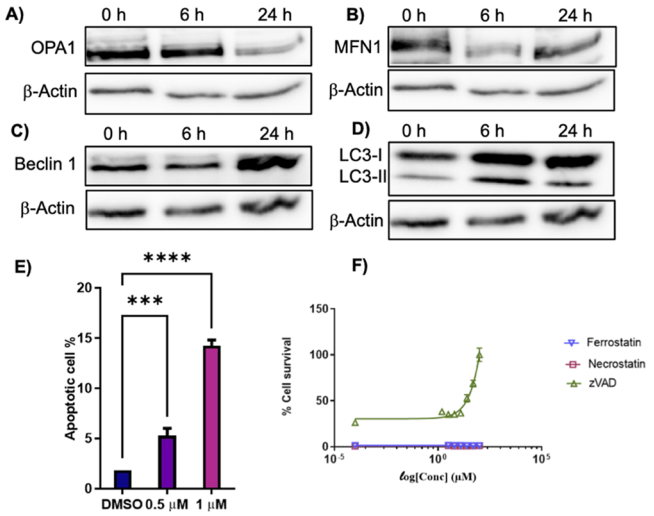

Figure 6. (A) Western blot analysis showing the effect of **Au-Mac1** on OPA1 expression in MDA-MB-468 cells (B) Western blot analysis showing the effect of **Au-Mac1** on MFN1 expression in MDA-MB-468 cells (C) Immunoblotting to monitor the expression of mitophagy marker. (D) Immunoblotting to monitor the expression of autophagy marker (E) Flow cytometry analyses of the apoptotic effect of **Au-Mac1** on MDA-MB-468 cells. Data are plotted as the mean ± SEM ($n = 3$). Data were analyzed by two-way ANOVA ($*p < 0.05$, $**p < 0.01$, $***p < 0.001$, $****p < 0.0001$. n.s., not significant) (F) Cell titer glo analyses of the effect of cell death suppressors Ferrostatin, Necrostatin and zVAD (Data plotted as the mean ± SD ($n = 3$).

immunoblotting to monitor the expression of autophagy markers (light chain protein 3) LC3-I and LC3-II as well as the mitophagy marker Beclin 1 (Figure 6C, D). **Au-Mac1**-induced expression of LC3-II/LC3-I represents an autophagic response. The autophagy protein Beclin 1 is critical in autophagosome formation, mitofusin degradation, and mitophagy initiation. Evidence for time-dependent Beclin 1 expression upon 1 μM **Au-Mac1** treatment suggests the onset of autophagy/mitophagy as an important cell death pathway (Figure 6C). Cell cycle studies in both MDA-MB-231 and MDA-MB-468 cells showed cell-specific responses to **AuMac1** treatment, inducing G1 arrest by 24 h in MDA-MB-231 cells or 6 h in MDA-MB-468 cells (Figures S44−50). To evaluate the extent of apoptosis induced by **Au-Mac1**, an Annexin V/PI dual staining assay was used to detect cells undergoing early and late-stage apoptosis. A significant population of cells treated with **Au-Mac1** undergoes apoptosis (Figures 6E, S51 and 52). Moreover, the dose-dependent effects of cell death suppressors (Ferrostatin −1: Ferroptosis inhibitor, Necrostatin-1: Necrosis inhibitor, and zVAD: Apoptosis inhibitor) on MDA-MB-468 cells treated with a lethal concentration (4 μM) of **Au-Mac1** were analyzed using Cell Titer Glo assay (Figure 6F). The cell survival plot revealed that zVAD inhibits cell death, indicating apoptosis as a dominant cell death pathway.

In Vivo Anticancer Activity of AuMac1. The in vivo efficacy of **Au-Mac1** was assessed in a BALB/c mouse model. We established a syngeneic model via subcutaneous implantation of 4T1 cells. 4T1 is a metastatic TNBC of mouse origin that provides an immunocompetent background to study drug efficacy. **Au-Mac1** was administered at 10 mg/kg via intraperitoneal (IP) injection three times per week (Figure

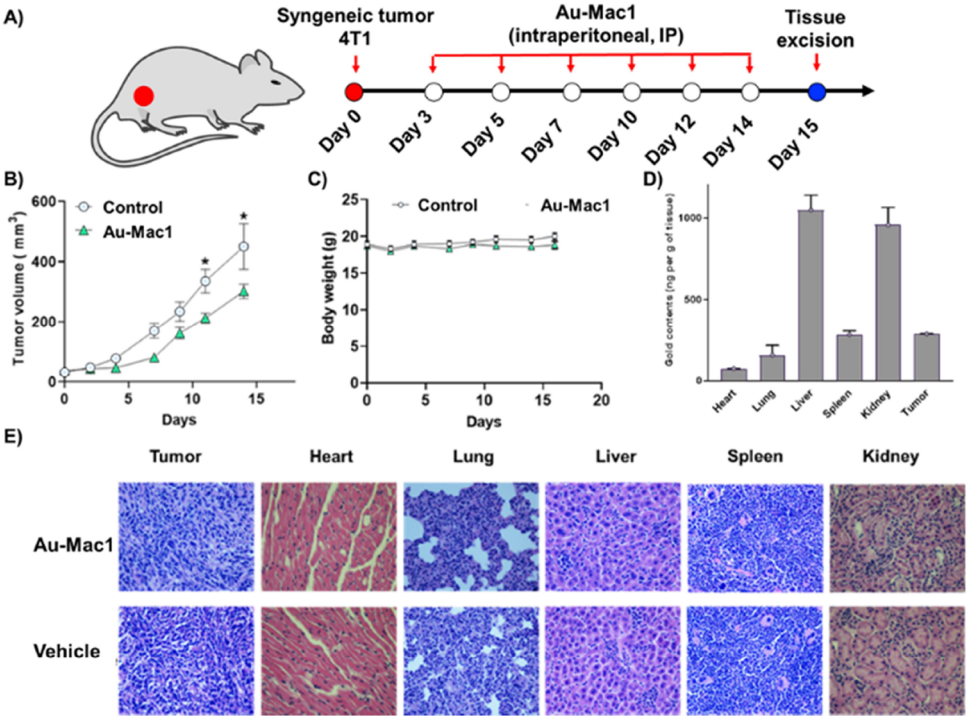

Figure 7. (A) Schematic representation of the in vivo efficacy study of **Au-Mac1** in a BALB/c mouse model. (B) In vivo tumor growth inhibition measured by tumor volume (C) Tolerability of **Au-Mac1** measured by body weight (Data plotted as mean ± SEM, $n = 4$ mouse per group, Two-sided Student's t test, p values are relative to vehicle control; $* 0.01 \leq p < 0.05$ (D) Biodistribution of complex **Au-Mac1,** Quantification of gold concentration in organ tissue measured using GF-AAS ($n = 2$) (E) Hematoxylin and eosin staining of different organ tissues of **Au-Mac1** treated and untreated mouse.

https://doi.org/10.1021/acs.jmedchem.4c02952
J. Med. Chem. XXXX, XXX, XXX−XXX

7A). A significant decrease was observed in the tumor volume after 12 days of treatment, and there was no significant change in the body weight between treated and control mice, indicative of enhanced in vivo efficacy and tolerability of **Au-Mac1** (Figure 7B, C).

Furthermore, the tissue biodistribution of **Au-Mac1** was analyzed in different organs of the treated mice. Drug biodistribution provides information on complex accumulation and elucidates drug metabolism and potential side effects. The highest content of gold was found in the kidney and liver (Figure 7D), suggesting a possible clearance pathway via these organs. Hematoxylin and eosin staining was performed to evaluate the cellularity of cancer tissue and preliminary toxicity in different organs. H & E staining revealed that the tumor proliferation was reduced in treated tumor tissue and other tissues did not show any difference in treated vs control tissue (Figure 7E). Overall, **Au-Mac1** inhibits metastatic 4T1 TNBC in mice with significant tolerability and reduced adverse effects.

CONCLUSIONS

In summary, we rationally designed and synthesized a novel class of organometallic Au(III) macrocycles bearing bis-phosphine ligands. Single crystal X-ray studies support a structure with a square planar geometry with the phosphines in a trans configuration. Comprehensive solution stability studies using LC-ESI-MS in cell medium, GSH, and blood serum support a stable class of metal complexes and are biocompatible for translational investigation in whole animals. The complexes display superior anticancer potency in triple-negative breast cancer cells (TNBC) with **Au-Mac1** having IC_{50}s in the range 480−630 nM. The cationic character of the complexes prompted mitochondrial investigations, which showed that **Au-Mac1** promotes ROS generation and induces mitochondrial membrane depolarization in TNBC. To identify the molecular target of **Au-Mac1**, we leveraged the carbonyl functionality to append a carboxylic acid group via oxime coupling and subsequent biotinylation to generate **Au-Mac1**-biotin. With this probe in hand, protein capture studies involving streptavidin pull-down were conducted and enriched proteins were analyzed by LC-MS/MS. HMOX2 was identified as the dominant target of **Au-Mac1**. Further validation studies using the CETSA and other functional molecular biology experiments verified the identified target. Additionally, **Au-Mac1** inhibits TNBC tumor growth in the 4T1 syngeneic murine model. We believe this work unveils a new strategy to utilize metal-based drugs to disrupt cellular-mitochondrial homeostasis and inhibit cancer growth.

METHODS

Materials and Methods. All of the reagents and solvents used in this work were bought from commercial vendors (Acros, Millipore-Sigma, TCI-America, Alfa Aesar, and Pharmco Aaper USA) and were used without additional purification unless explicitly stated otherwise. $HAuCl_4{\cdot}3H_2O$ was purchased from NANOPARTZ and stored in a glovebox or desiccator before use. 2-benzoylpyridine, 2-benzylpyridine, 2-phenylpyridine, 2-phenoxypyridine, and Benzo[h]quinoline ligands were purchased from the following commercial vendors Sigma-Aldrich, TCI America, and Alfa Aesar. (R,R)-DACH phenyl Trost ligand was purchased from Santa Cruz. Deuterated solvents for NMR were acquired from Cambridge Isotope Laboratories and used as is. Compounds were purified by silica gel (SiliCycle, P/N: R10030B SiliaFlash F60, size: 40−63 μm, Canada) for column chromatography. Analytical thin-layer chromatography (TLC) was performed by aluminum-backed silica-gel plates (20 × 20 cm^2, TLA-R10011B-323) from SiliCycle. Reactions were conducted under standard atmospheric conditions. Progress of the reactions was evaluated by NMR and TLC. Low-wavelength light (254 nm) was used to visualize the TLC plates. The purity of the compounds synthesized was ascertained by HPLC with purity >95%.

Physical Measurements. ^{1}H NMR and $^{13}C\{^1H\}$ NMR spectra were collected on a 500 MHz Bruker spectrometer, a 400 MHz Varian spectrometer, or a 500 MHz JEOL ECZr at the University of Kentucky (UK) NMR Center. Solvent signals were used as internal reference (^{1}H NMR: DMSO at δ = 2.50 ppm and CD_3OD at δ = 3.31; ^{13}C NMR: DMSO at δ = 39.52 ppm and CD_3OD at δ = 49.00 ppm) for chemical shifts in the ^{1}H NMR spectra collected. X-ray crystal structures were obtained from the UK X-ray crystallography center at the Department of Chemistry. Synergy H1 hybrid plate reader at the College of Pharmacy (UK) was used for the cell viability experiment. Flash silica-gel chromatography was performed using Combi-Flash from Teledyne ISCO. An Agilent 1100 series HPLC instrument connected to Advion (reverse-phase C18 column) was used to obtain the trace HPLC data and low-resolution ESI -MS spectrum. Flow cytometry data were obtained from UK flow cytometry and immune monitoring core facility using CytoFLEXLX. Mitochondrial bioenergetics were studied using a UK RM SRF core facility using a Seahorse XFe96 analyzer.

Synthetic Procedures. Synthesis of cyclometalated gold(III) complexes. [(C^N)Au(III)-(pcp) Cl_2][pcp = 2-(2-pyridylcarbonyl)-phenyl], [(C^N)Au(III)-(byp)Cl_2][byp = 2-benzylpyridine], (C^N)-phenyl,2-pyridyl ether-Au(III)Cl_2, [(C^N)Au(III)-(PhPy) Cl_2][PhPy = 2-phenylpyridine] and [(C^N)Au(III) -benzo(h) quinoline-Cl_2] were synthesized using a heating mantle equipped with pressure tube using high temperature of ∼270 °C as previously reported.

Synthesis of ***Au-Mac1****.* To a 25 mL round-bottom flask were added [C^N] Au(III)- (pcp) Cl_2] (mg, mmol), (R,R)-DACH phenyl Trost ligand (69.4 mg, 0.2 mmol, 2 equiv), and 10.0 mL of MeOH/DCM (v/v = 1:1) and the mixture stirred for 2−4 h at room temperature. A pale-yellow clear solution was formed. The progress of the reaction was monitored by using TLC. The solvent was evaporated in vacuo and the crude was redissolved in a minimal amount of DCM and precipitated with diethyl ether. (yield = 80%). ^{1}H NMR (400 MHz, $CDCl_3$-*d*) δ 9.16 (s, 1H), 9.10−9.06 (m, 1H), 8.54 (d, *J* = 7.8 Hz, 1H), 8.44 (d, *J* = 7.7 Hz, 1H), 8.34 (d, *J* = 4.7 Hz, 1H), 8.28 (d, *J* = 7.9 Hz, 1H), 7.63−7.50 (m, 5H), 7.46 (d, *J* = 7.6 Hz, 2H), 7.35 (d, *J* = 7.6 Hz, 2H), 7.14 (d, *J* = 7.2 Hz, 2H), 7.02 (dt, *J* = 26.5, 8.0 Hz, 5H), 6.92−6.81 (m, 4H), 6.76−6.61 (m, 7H), 6.36−6.29 (m, 1H), 5.28 (d, *J* = 10.4 Hz, 1H), 3.87 (s, 1H), 1.97 (t, *J* = 12.7 Hz, 2H), 1.70 (s, 2H), 1.60 (d, *J* = 12.2 Hz, 1H), 1.48 (d, *J* = 12.7 Hz, 1H), 1.35 (t, *J* = 12.7 Hz, 1H).^{31}P $\{^1H\}$ NMR (162 MHz, $CDCl_3$-*d*) δ 35.97, 35.68.^{13}C $\{^1H\}$ NMR (101 MHz, $CDCl_3$-*d*) δ 194.36, 165.81, 165.45, 153.92, 147.63, 135.90, 135.29, 132.65, 132.44, 132.26, 131.13, 131.00, 130.04, 129.81, 128.16, 125.64, 124.78, 124.47, 77.33, 77.01, 76.69, 55.89, 50.76, 33.64, 30.94, 25.32.MS - ES^+ - API: *m*/*z*, *z* = 2 (%) 552.9 (100), calculated *m*/*z*, *z* = 2 for [M^+] 552.12 (100). Elemental anal. % Calculated for $C_{56}H_{48}AuCl_2N_3O_3P_2{\cdot}0.05\ CH_2Cl_2$: C, 58.79%; H, 4.23%; N, 3.67%. Found: C, 58.51%; H, 4.53%; N, 3.64%.HPLC method. Flow rate: 1 mL/min; λ = 260 nm; Eluent A = H_2O with 0.1% TFA; Eluent B = ACN with 0.1% Formic acid; Solvent Gradient: 0−15 min (0:100 H_2O: ACN), 5 min (100:0 H_2O: ACN).

Synthesis of ***Au-Mac2****.* The same procedure from the synthesis of **Au-Mac1** was followed using (C^N) 2-phenoxypyridine -Au (III)Cl_2. (yield = 78%).^{1}H NMR (400 MHz, $CDCl_3$-*d*) δ 9.32 (d, *J* = 8.9 Hz, 1H), 8.94 (d, *J* = 6.4 Hz, 1H), 8.60−8.53 (m, 1H), 8.47−8.41 (m, 1H), 7.76 (d, *J* = 8.0 Hz, 1H), 7.67−7.51 (m, 4H), 7.43−7.34 (m, 2H), 7.35−7.27 (m, 5H), 7.14 (t, *J* = 7.6 Hz, 3H), 7.06−6.87 (m, 9H), 6.80−6.65 (m, 8H), 6.47 (td, *J* = 8.2, 4.4 Hz, 1H), 5.30 (td, *J* = 10.5, 9.9, 3.4 Hz, 1H), 3.93 (p, *J* = 7.2 Hz, 1H), 3.46 (s, 2H), 1.75−1.62 (m, 3H), 1.54−1.34 (m, 2H).^{31}P $\{^1H\}$ NMR(162 MHz, $CDCl_3$-*d*) δ 35.09, 34.87. ^{13}C $\{^1H\}$ NMR (101 MHz, $CDCl_3$-*d*) δ: 166.09, 165.36, 161.72, 154.34, 146.99, 138.31, 137.83, 136.92, 135.18, 134.84, 134.19, 133.70, 132.45, 132.39, 131.22, 130.17, 129.98, 128.89, 128.09, 127.74, 127.73, 126.56, 119.59, 118.08, 112.23, 77.32,

https://doi.org/10.1021/acs.jmedchem.4c02952
J. Med. Chem. XXXX, XXX, XXX−XXX

77.00, 76.69, 55.88, 50.65, 33.47, 30.77, 25.29. MS - ES$^+$ - API: *m/z*, *z* = 2 (%) 546.10 (100), calculated *m/z*, *z* = 2 for [M$^+$] 546.12 (100). Elemental Anal. % Calcd for $C_{55}H_{48}AuCl_2N_3O_3P_2 \cdot 1.05\ CH_2Cl_2$: C, 55.27%; H, 4.15%; N, 3.45%. Found: C, 55.1%; H, 4.35%; N, 3.44%.HPLC method. Flow rate: 1 mL/min; λ = 260 nm; Eluent A = H_2O with 0.1% TFA; Eluent B = ACN with 0.1% Formic acid; Solvent Gradient: 0−15 min (0:100 H_2O: ACN), 15−20 min (100:0 H_2O:ACN).

*Synthesis of **Au-Mac3**.* The same procedure from the synthesis of **Au-Mac1** was followed using (C^N) 2-phenylpyridine -Au(III)Cl_2. (yield = 76%). ^{1}H NMR (500 MHz, $CDCl_3$-*d*) δ 9.39 (d, *J* = 8.9 Hz, 1H), 8.94 (d, *J* = 6.2 Hz, 1H), 8.74 (s, 1H), 8.61 (d, *J* = 7.9 Hz, 1H), 8.46 (d, *J* = 7.8 Hz, 1H), 8.29 (s, 1H), 7.92 (d, *J* = 8.0 Hz, 1H), 7.65 (dt, *J* = 16.1, 7.5 Hz, 3H), 7.46 (dt, *J* = 14.7, 7.3 Hz, 4H), 7.40 (t, *J* = 7.1 Hz, 2H), 7.33 (q, *J* = 8.2 Hz, 4H), 7.27 (s, 1H), 7.22 (t, *J* = 7.5 Hz, 2H), 6.97 (ddt, *J* = 26.7, 17.5, 7.6 Hz, 7H), 6.85 (t, *J* = 7.6 Hz, 1H), 6.72−6.67 (m, 2H), 6.61 (dd, *J* = 14.9, 7.0 Hz, 5H), 6.42 (d, *J* = 8.6 Hz, 2H), 5.77 (d, *J* = 7.7 Hz, 1H), 5.28−5.23 (m, 1H), 3.93 (tt, *J* = 11.4, 5.9 Hz, 1H), 3.37 (d, *J* = 16.3 Hz, 1H), 3.01 (s, 1H), 1.77−1.60 (m, 4H), 1.55−1.43 (m, 1H), 1.40−1.18 (m, 4H), 0.86 (dt, *J* = 19.2, 6.3 Hz, 1H). ^{31}P {^{1}H} NMR (202 MHz, $CDCl_3$-*d*) δ 33.62, 33.53. ^{13}C {^{1}H} NMR (101 MHz, $CDCl_3$-*d*) δ: 166.03, 165.35, 139.13, 138.53, 137.88, 136.46, 136.35, 135.22, 134.87, 134.82, 133.64, 133.23, 132.57, 131.75, 131.12, 130.38, 130.04, 128.95, 128.32, 128.08, 127.48, 126.49, 77.31, 77.00, 76.68, 55.88, 50.67, 33.40, 30.66, 25.24, 25.20. MS - ES$^+$ - API: *m/z*, *z* = 2 (%) 545.30 (100), calculated *m/z*, *z* = 2 for [M$^+$] 545.13 (100). Elemental Anal. % Calcd for $C_{56}H_{50}AuCl_2N_3O_3P_2 \cdot 0.65\ C_4H_{10}O$: C, 59.1%; H, 4.78%; N, 3.53%. Found: C, 59.18%; H, 4.89%; N, 3.64%. HPLC method. Flow rate: 1 mL/min; λ = 260 nm; Eluent A = H_2O with 0.1% TFA; Eluent B = ACN with 0.1% Formic acid; Solvent Gradient: 0−15 min (0:100 H_2O: ACN), 5 min (100:0 H_2O:ACN).

*Synthesis of **Au-Mac4**.* The same procedure from the synthesis of **Au-Mac1** was followed using (C^N) 2-benzylpyridine -Au(III)Cl_2. Silica gel flash column chromatography (eluent 0−5% DCM in MeOH) was used to purify the complex. (yield = 37%). ^{1}H NMR (400 MHz, $CDCl_3$ *d*) δ 9.13 (d, *J* = 6.2 Hz, 1H), 8.93 (d, *J* = 8.8 Hz, 1H), 8.58−8.37 (m, 3H), 7.56 (dq, *J* = 14.3, 7.4 Hz, 4H), 7.31 (d, *J* = 7.6 Hz, 1H), 7.25−7.15 (m, 6H), 7.07 (td, *J* = 7.7, 1.8 Hz, 2H), 7.03−6.87 (m, 10H), 6.79 (s, 1H), 6.70 (t, *J* = 6.3 Hz, 1H), 6.45 (dt, *J* = 27.0, 8.5 Hz, 3H), 6.09 (ddd, *J* = 10.4, 7.4, 2.4 Hz, 1H), 3.90 (d, *J* = 6.3 Hz, 1H), 2.19 (s, 4H), 1.97 (t, *J* = 13.1 Hz, 2H), 1.84 (td, *J* = 12.5, 3.5 Hz, 1H), 1.70 (d, *J* = 22.7 Hz, 2H), 1.64−1.55 (m, 1H), 1.55−1.42 (m, 1H), 1.42−1.25 (m, 2H). ^{31}P {^{1}H} NMR (162 MHz, $CDCl_3$ - *d*) δ: 34.73, 33.63. ^{13}C {^{1}H} NMR (101 MHz, $CDCl_3$-*d*) δ: 165.68, 165.41, 147.62, 138.19, 137.25, 135.93, 135.00, 133.14, 132.37, 132.11, 131.94, 130.76, 130.54, 130.42, 129.94, 129.89, 129.53, 128.27, 128.20, 128.06, 128.00, 127.19, 127.10, 126.42, 121.68, 77.30, 76.98, 76.67, 55.83, 53.38, 50.89, 33.55, 30.86, 25.39, 25.28. MS - ES$^+$ - API: *m/z*, *z* = 2 (%) 538.20 (100), calculated *m/z*, *z* = 2 for [M$^+$] 538.13 (100).

*Synthesis of **Au-Mac5**.* The same procedure from the synthesis of **Au-Mac1** was followed using (C^N) 2-benzo(h)quinoline -Au(III)-Cl_2. Silica gel flash column chromatography (eluent 0−5% DCM in MeOH) was used to purify the complex. (yield = 28%). ^{1}H NMR (400 MHz, $CDCl_3$ *d*) δ 9.17 (d, *J* = 8.8 Hz, 1H), 8.91 (dd, *J* = 29.2, 7.8 Hz, 3H), 8.52−8.44 (m, 3H), 8.27−8.13 (m, 2H), 7.93 (s, 1H), 7.83−7.63 (m, 4H), 7.63−7.54 (m, 6H), 7.38 (ddd, *J* = 35.2, 12.3, 5.2 Hz, 10H), 7.19 (dd, *J* = 15.6, 6.0 Hz, 4H), 7.08 (d, *J* = 7.3 Hz, 2H), 7.00 (q, *J* = 7.8 Hz, 2H), 6.93−6.81 (m, 2H), 6.77−6.54 (m, 8H), 6.40 (t, *J* = 9.1 Hz, 2H), 6.00 (d, *J* = 41.7 Hz, 5H), 5.33−5.28 (m, 1H), 3.94 (s, 1H), 1.96 (d, *J* = 13.9 Hz, 4H), 1.71 (d, *J* = 12.0 Hz, 3H), 1.58 (s, 1H), 1.44−1.28 (m, 2H), 1.21 (s, 1H). ^{31}P {^{1}H} NMR (162 MHz, $CDCl_3$ - *d*) δ 31.98, 31.74, 30.20, 30.01. ^{13}C {^{1}H} NMR (101 MHz, $CDCl_3$-*d*) δ: 165.76, 165.23, 165.20, 148.60, 137.90, 135.57, 134.99, 134.30, 132.36, 132.31, 131.84, 131.68, 131.09, 130.94, 130.78, 129.86, 129.74, 128.78, 128.72, 128.15, 128.08, 127.41, 126.83, 126.26, 125.61, 124.95, 124.41, 120.80, 120.37, 77.29, 76.97, 76.65, 55.78, 53.37, 51.06, 33.44, 30.60, 25.45, 25.33.

*Synthesis of [C^N]Au(III)-(pcp) Cl2][pcp = 2-(2-Pyridylcarbonyl)-phenyl] (**S1**).* To a 25 mL round-bottom flask, a solution of $HAuCl_4 \cdot 3H_2O$ (0.200 g, 1 mmol, 1 equiv) in DI water (10 mL) was added phenyl(pyridin-2-yl)methanone (0.102 g, 1 mmol, 1 equiv). The solution was placed in a pressure tube for 48 h. After 48 h, the reaction mixture was filtered under vacuum and the precipitate was washed with DI water, ethanol, and diethyl ether. White solid product was obtained (yield = 63%). ^{1}H NMR (500 MHz, DMSO-D_6) δ 9.48 (d, *J* = 4.7 Hz, 1H), 8.55 (t, *J* = 7.7 Hz, 1H), 8.37 (d, *J* = 9.6 Hz, 1H), 8.09 (t, *J* = 7.7 Hz, 1H), 7.76 (d, *J* = 7.4 Hz, 1H), 7.69 (dd, *J* = 6.9, 2.5 Hz, 1H), 7.51−7.43 (m, 2H).^{13}C NMR (126 MHz, DMSO-D_6) δ 189.24, 153.33, 145.67, 144.88, 137.26, 134.48, 133.76, 130.42, 130.11, 129.12, 128.32, 127.63

*Synthesis of Au(III) Oxime (**S2**).* To a 25 mL round-bottom flask was added a solution of [C^N]Au(III)-(pcp) Cl_2] (80 mg, 0.2 mmol 1 equiv) in DCM (5 mL) and Methanol (5 mL) and (Aminooxy) acetic acid hemihydrochloride (49 mg, 0.6 mmol, 3 equiv). The solution was placed in a 20 mL vial and stirred for 48 h at RT. After 48 h, the reaction mixture was filtered under vacuum and the precipitate was washed with Methanol 3 times. A white solid product was obtained. (yield = 67%). ^{1}H NMR (500 MHz, DMSO-d6) δ 9.31 (d, *J* = 6.0 Hz, 1H), 8.46 (d, *J* = 4.3 Hz, 2H), 7.93 (q, *J* = 5.0 Hz, 1H), 7.51 (d, *J* = 8.0 Hz, 1H), 7.34−7.23 (m, 3H), 4.89 (s, 2H). ^{13}C NMR (126 MHz, DMSO-d6) δ: 171.11, 153.50, 153.26, 144.24, 143.83, 137.99, 133.87, 130.51, 129.19, 129.04, 128.69, 128.28, 128.12, 72.19.

*Synthesis of Oxime-biotin-EDA (**S3**).* To a well-purged Schlenk flask biotin, EDA (27.2 mg, 0.095 mmol), oxime (24.8 mg, 0.047 mmol), HOBt (19.34 mg, 0.14 mmol), and EDC (27.46 mg, 0.14 mmol) in 1.0 mL of anhydrous DMF was added and stirred overnight at RT. The progress of the reaction was monitored by using TLC. After 24 h, water (10 mL) was added and extracted from the DCM/IPA mixture (1:1). Organic layers were washed with 30.0 mL of brine and dried over anhydrous $MgSO_4$. The solvent was evaporated *in vacuo*. Yield: 25 mg, 33%. ^{1}H NMR (400 MHz, DMSO-d6) δ 9.35 (dd, *J* = 6.0, 1.5 Hz, 1H), 8.70 (dd, *J* = 8.0, 1.6 Hz, 1H), 8.50 (td, *J* = 7.8, 1.5 Hz, 1H), 8.24 (t, *J* = 5.3 Hz, 1H), 8.01−7.92 (m, 3H), 7.73 (dt, *J* = 8.3, 1.0 Hz, 1H), 7.55 (ddd, *J* = 8.3, 5.4, 1.1 Hz, 2H), 7.44−7.41 (m, 1H), 7.38−7.34 (m, 2H), 7.34 (s, 1H), 6.43−6.35 (m, 2H), 4.77 (s, 2H), 4.29 (dd, *J* = 7.7, 5.0 Hz, 1H), 4.13−4.07 (m, 1H), 3.21 (dt, *J* = 14.2, 5.6 Hz, 4H), 3.09−3.02 (m, 1H), 2.80 (dt, *J* = 12.4, 5.3 Hz, 1H), 2.56 (d, *J* = 12.4 Hz, 1H), 2.07 (t, *J* = 7.4 Hz, 2H), 1.48 (h, *J* = 3.8 Hz, 2H), 1.29 (s, 1H). ^{13}C NMR (101 MHz, DMSO-d6) δ 172.36, 167.94, 162.50, 152.44, 143.91, 142.86, 137.22, 137.09, 133.06, 130.95, 130.05, 129.73, 128.20, 127.48, 127.18, 124.33, 118.95, 109.40, 73.65, 60.79, 58.97, 55.63, 55.17, 39.94, 39.73, 39.52, 39.31, 39.10, 38.89, 38.69, 37.99, 34.99, 27.97, 27.81, 24.96. HRMS (ESI) (*m/z*): calcd for $C_{26}H_{31}AuCl_2N_6O_4S$ [M]$^+$, 790.1170; found [M + H], 791.1240 Δ = −1.007.

*Synthesis of **AuMac1**-biotin Probe.* To a 25 mL round-bottom flask, gold(III) oxime biotin (44.5 mg, 0.056 mmol), (R,R) − DACH phenyl Trost ligand (38.8 mg, 0.056 mmol) and DCM/MeOH (v/v = 1:1) was added and stirred at rt. The progress of the reaction was monitored by using TLC. After 2 h, all the ligand was consumed. The solvent was evaporated *in vacuo*. Flash column chromatography (0-10% MeOH in DCM) was used to purify the product. Yield: 30 mg, 58%. Rf = 0.2 (DCM/MeOH, 10:1). ^{1}H NMR (400 MHz, $CDCl_3$) δ 9.53 (s, 1H), 8.65 (s, 2H), 8.51 (d, *J* = 12.5 Hz, 3H), 8.19 (s, 1H), 7.69 (t, *J* = 7.5 Hz, 2H), 7.64−7.51 (m, 9H), 7.45 (d, *J* = 7.5 Hz, 2H), 7.34 (dt, *J* = 15.4, 7.6 Hz, 8H), 7.20 (t, *J* = 7.6 Hz, 4H), 7.10 (s, 3H), 7.00 (d, *J* = 20.0 Hz, 6H), 6.82 (d, *J* = 8.5 Hz, 5H), 6.68 (q, *J* = 7.0 Hz, 4H), 6.58 (t, *J* = 7.0 Hz, 4H), 6.34 (s, 3H), 5.99−5.88 (m, 5H), 5.28 (d, *J* = 14.8 Hz, 2H), 4.47 (s, 1H), 4.29 (s, 2H), 4.12 (q, *J* = 7.1 Hz, 1H), 3.98 (d, *J* = 16.1 Hz, 3H), 3.85 (d, *J* = 16.7 Hz, 2H), 3.42 (d, *J* = 46.5 Hz, 7H), 3.13 (s, 1H), 2.87 (d, *J* = 12.4 Hz, 2H), 2.27 (s, 3H), 1.93 (s, 5H), 1.70 (s, 7H), 1.55 (d, *J* = 11.5 Hz, 4H), 1.46 (d, *J* = 7.2 Hz, 3H), 1.33 (d, *J* = 3.3 Hz, 4H). ESI-MS *m/z* (positive mode): calcd for [M − Cl]$^+$ $C_{70}H_{71}AuClN_8O_6P_2S$ 1445.40, found 723.30 ([M − Cl]$^+$/2).

X-ray Crystallography. A Bruker D8 Venture dual-source diffractometer was used to collect the low-temperature (90 K) X-

https://doi.org/10.1021/acs.jmedchem.4c02952
J. Med. Chem. XXXX, XXX, XXX−XXX

ray diffraction data of **Au-Mac1**, and **Au-Mac2**, and a summary of the crystallographic information is reported in Tables S1 and S2. Complexes **Au-Mac1** and **Au-Mac2** were dissolved in a minimal amount of $CHCl_3$, and diethyl ether was used to grow the crystals at room temperature by the vapor diffusion method. All crystals were mounted by using polyisobutene oil on the tip of a fine glass fiber, which was fastened in a copper mounting pin with an electrical solder. Mounted crystals were placed directly into the cold gas stream of a liquid nitrogen-based cryostat. The APEX3 package was used for Lorentz polarization effects such as raw data integration, scaling, merging, and correction. SHELXT and SHELXL were used respectively to determine the space group and refinement. Refinement of nonhydrogen atoms was performed by using anisotropic displacement parameters. Hydrogen atoms were placed at calculated positions and refined by using a riding model with their isotropic displacement parameters (Uiso) set to either 1.2Uiso or 1.5Uiso of the atom to which they were attached. The graphical program SHELXTL-XP was used to draw the ellipsoid plots. All the structures were checked for missed symmetry, twinning, and overall quality with PLATON, an R-tensor before submitting to the Cambridge Structural Database (CSD). Finally, CheckCIF was used for the validation of the structures.

Stability of Complexes in Biologically Relevant Media. Complexes **Au-Mac1, Au-Mac2,** and **Au-Mac3** were dissolved in a minimal amount of CH_3CN and diluted with biologically relevant media DMEM and RPMI, respectively, to make the final concentration of the complexes ∼0.7 mM (1 mg/mL) in 1.0 mL media. At each time point (0, 4, 8, 12, and 24 h), 20 μL of the incubated solution (complex and media) was injected into LC/ESI-MS to record the HPLC chromatogram and mass spectrum. The complex mixture was incubated at 37 °C between injections. The parameters used in the HPLC were as follows: flow rate, 1 mL/min; λ = 280 nm; eluent A = H_2O with 0.1% TFA; Eluent B = CH_3CN with 0.05% HCOOH; Solvent gradient: 0 min (100:0 H_2O:CH_3CN), 10 min (0:100 H_2O:CH_3CN), 15 min (100:0 H_2O:CH_3CN).

Reaction with L-Glutathione (GSH). One mg portion of the compound was dissolved in 200 μL of CH_3CN and diluted with water to make 500 μL. (1.8 mM). 1.8 mM stock solution of GSH was made by dissolving the GSH in pure water. An equal volume of compound solution and GSH solution was mixed and maintained the complex: GSH = 1:1 ratio. Reaction mixtures were incubated at 37 °C in between each run. One milligram of the compound was dissolved in 200 μL of CH_3CN and diluted with water to make 500 μL. (1.8 mM). Eighteen mM stock solution of GSH was made by dissolving the GSH in pure water. An equal volume of compound solution and GSH solution was mixed and maintained the complex: GSH = 1:10 ratios. The LC/ESI-MS was recorded at each time point 0, 1, 4, 6, 12 and 24 h. The parameters used in the HPLC were as follows: flow rate, 1 mL/min; λ = 280 nm; eluent A = H_2O with 0.1% TFA; Eluent B = CH_3CN with 0.05% HCOOH; Solvent gradient: 0 min (100:0 H_2O:CH_3CN), 10 min (0:100 H_2O:CH_3CN), 15 min (100:0 H_2O:CH_3CN).

Mouse Serum Stability Test. Three female BALB/cJ mice (5 weeks) were received from the Jackson Laboratory (Bar Harbor, ME), and they had an acclimation period of 1 week. After 9 weeks, serum was collected from the mice. After aliquoting the serum, **Au-Mac1** in DMSO (1 mM) was added to each sample and incubated at 37 °C. At varying time points (0, 10, 30, 60, 120, 360, and 1440 min) methanol was added to each sample and vortexed for 1 min at room temperature. And centrifuged to separate the phases. Only supernatant was taken and analyzed by LC/ESI-MS. Two samples were measured at each time point. Peaks of the HPLC chromatogram were calculated at each time point. The parameters used in the HPLC were as follows: flow rate, 1 mL/min; λ = 280 nm; eluent A = H_2O with 0.1% TFA; Eluent B = CH_3CN with 0.05% HCOOH; Solvent gradient: 0 min (100:0 H_2O:CH_3CN), 10 min (0:100 H_2O:CH_3CN), 15 min (100:0 H_2O:CH_3CN).

Cell Culture. MDA-MB-231, MDA-MB-468, MDA-MB-436, SUM159, and Hs578T cell lines were purchased from ATCC. MDA-MB-231, MDA-MB-468, and MDA-MB-436 cells were cultured in Dulbecco's modified Eagle's medium (DMEM) supplemented with 10% FBS, 1% penicillin/streptomycin, and 1% amphotericin. SUM159 cells were cultured in DMEM/F12 with penicillin/streptomycin/L-glutamine and 10% fetal bovine serum supplemented with 5 mg/mL insulin. Hs578T cells were cultured in high glucose DMEM with 10 mg/mL insulin, penicillin/streptomycin/L-glutamine, and 10% fetal bovine serum.

All cells were maintained at 37 °C in a humid atmosphere with 5% CO_2. PBS and trypsin-EDTA used for cell culture maintenance were also purchased from Corning Inc. and used as purchased.

Cell Viability Assay. Various cells (MDA-MB-231, MDA-MB-468, MD-MB-436, SUM159, H_S578T) (3×10^3) were seeded in each well of a 96-well plate. After the cells were incubated overnight at 37 °C, various concentrations of test compounds **Au-Mac1, Au-Mac2, Au-Mac3, Au-Mac4, Au-Mac5,** and **ligand** (0.13−100 μM) were added and incubated for 72 h (total volume of 200 μL). After 72 h incubation, media was removed and 100 μL of 0.5 mg/mL MTT solution was added to each well in the darkness to protect the MTT from light. Plates were incubated for 3.5 h at 37 °C and MTT solution was removed from each well. 100 μL of DMSO was added to each well, and plates were read using a plate reader (Absorbance 570 nm). For ovarian cancer cells, treatment conditions were the same, except that Cell Titer Glo was used for the assay.

TMRE Assay. MDA-MB-468 cells were seeded at a density of 5×10^5 cells/well in a six-well plate and allowed to adhere overnight at 37 °C. **Au-Mac1** was prepared as a stock in DMSO and treated at final concentrations of 5 and 10 μM after dilution in DMEM. The cells were incubated at 37 °C (5% CO_2) for 2 h. For positive control, carbonyl cyanide 3-chlorophenylhydrazone (CCCP) was prepared as a stock in DMSO and added at a final concentration of 100 μM for 1 h. After the incubation time, the cells were trypsinized, pelleted by centrifugation, and resuspended in 200 μL of TMRE dye solution (200 nM) at room temperature for 20 min. After the incubation time, cells were centrifuged, and the staining solution was removed and replaced with 200 μL of PBS. This was followed by analysis on a flow cytometer with a PE channel.

Cell Cycle Analysis. Cells (MDA-MB-468 and MDA-MB-231) (3×10^5) were seeded in each well of a six-well (20 wells) plate. After cells were incubated overnight, 0.5 μM **Au-Mac1** for 9 wells and 1 μM **Au-Mac1** for 9 wells were added, and 2 wells were kept without adding compounds and incubated at 37 °C. After 6 h of incubation, 3 wells per concentration were harvested via trypsinization and centrifuged to form a pellet. The pellet was washed with PBS, transferred to 1.5 mL centrifuge tubes, and centrifuged to form a pellet. Then the PBS was decanted, and the pellet was resuspended in 1.0 mL of 70% ethanol in PBS and stored at 4 °C. The same procedure was followed to collect the 12 and 24 h time points. A total of 50 μL of 100 μg/mL RNase solution and 200 μL of 50 μg/mL propidium iodide solution were added to each sample and resuspended and incubated in the ice for 30 min and cells were filtered via a strainer. All the samples were analyzed with flow cytometry.

Apoptosis Analysis. MDAMB468 cells (3×10^5) and MDAMB231 (2×10^5) were seeded in each well of a six-well (12 wells) plate. After the cells were incubated overnight, 0.5 μM of **Au-Mac1** for three wells, 1 μM **Au-Mac1** for three wells were added, and 0.5 μM of DMSO for one well and 200 μM of H_2O_2 for one well were added and three wells were kept without adding compounds and incubated for 48 h (total volume 2 mL). After 48 h, media was transferred to labeled 15.0 mL centrifuge tubes, washed with 1.0 mL PBS, and transferred to labeled centrifuge tubes. Cells were harvested via trypsinization and transferred to labeled centrifuge tubes. Tubes were centrifuged for 5 min to form a pellet. Pellets were washed with PBS twice, resuspended 500 μL of annexin binding buffer, and transferred to FACS tubes. Five μL of propidium iodide and 5 μL of annexin V-FITC were added to each tube and incubated in the dark for 5 min and analyzed with flow cytometry.

Evaluate the Dose-Dependent Effect of Cell Death Suppressing Compounds. 5000 cells per well (MDA-MB-468) were seeded in the white bottom 96-well plate and allowed to adhere overnight in an

https://doi.org/10.1021/acs.jmedchem.4c02952
J. Med. Chem. XXXX, XXX, XXX−XXX

incubator at 37 °C. Each well was treated with 25 μL of 4 μM (four times of IC_{50}) **Au-Mac1**. Plates were treated with serial dilution of 25 μL of ferrostatin- 1, necrostatin and zVAD − FMK (100, 50, 25, 12.5, 6.25, 3.13, 1.56, and 0 μM). After 24 h incubation, all the plates were kept at room temperature for 30 min. 60 μL of Cell Titer Glo luminescence solution was added to the desired wells. Using the plate reader plates were shaken orbitally for 2 min and then plates were allowed to rest for 10 min to stabilize. Luminescence was run scan with 1000 ms integration and 150 ms gain.

Mitochondrial Metabolism Analysis Using Seahorse XF96 Analyzer. 30,000 cells/well (optimized condition) MDA-MB-468 cells were plated. The cells were seeded the night prior to the experiment with a final volume of 100 μL and incubated overnight at 37 °C. **Au-Mac1** was prepared as a stock in DMSO and diluted to a working concentration of 200 μM with Seahorse XF96 assay buffer, and then subsequently serial dilutions were made to achieve multiple concentrations. The assay was performed using a pneumatic injection method of **Au-Mac1**, with the final injection concentrations of 0.1, 1, 3, and 10 μM. This was followed by injection of oligomycin (1.0 μM), FCCP (0.6 μM), and rotenone/antimycin A (0.5 μM). The same procedure was followed for the MDA-MB-231 cells.

Immunoblotting Assay. The cells were seeded in equal numbers and allowed to adhere and grow to 80% confluence, after which the cells were treated with **Au-Mac1** (1 μM) at different time points. At 6 and 24 h, cells were washed twice with PBS, then RIPA buffer was added, and cells were scraped and collected into 1.5 mL centrifuge tubes and kept. The mixture was centrifuged for 15 min at 14,000*g* and the supernatant was separated from the debris. The cell lysates with equal amounts of protein were reconstituted in Laemmli Buffer and heated at 90 °C for 10 min. The protein mixture was then separated by 4−20% SDS-polyacrylamide gel electrophoresis (35 min, 100 V) and transferred to a PVDF membrane (1 h, 350 mA). The membrane was then blocked with 5% (w/v) bovine serum albumin (BSA) in PBST for 1 h followed by incubation of the membranes with primary antibodies overnight at 4 °C. The following day, the membranes were washed three times with PBST and incubated with horseradish peroxidase-conjugated secondary antibodies (rt, 1 h) prepared in a BSA blocking solution. The membranes were washed with PBST (3× for 5 min) after incubation with a secondary antibody. The membranes were placed in pierce enhanced chemiluminescence substrate and visualized with a Bio-Rad imager. All antibodies used for this study were purchased from cell signaling technology. The primary antibodies are MFN1 (CST, #14739S), LC3 I/II (CST, #2775S), BECLIN-1 (CST, #3738S), OPA1, (CST, #80471S) and β-actin (CST, #3700S).

Pull-Down Protocol. MDA-MB468 cells were plated in DMEM at 1×10^6 cells per T25 (X6) cell culture flask and allowed to adhere overnight. After 24 h experiment, the flask was treated with 10 μM Au-Mac1-Biotin for 2 h. After 2 h, cells were scraped and collected into a 15 mL tube. Flasks were washed with 1 mL of cold PBS and transferred to their corresponding 15 mL tube. Cells were centrifuged, and pellets were resuspended with 1 mL of cold PBS and transferred into a 1.5 mL tube. This was followed by centrifugation at 2500*g* (4500 rpm) for 5 min at 4 °C. Decant supernatant, keep pelleted cells. The pellets were resuspended in 0.25 mL of RIPA buffer, after which the cells were sonicated (30 s pulses X2). The mixture was placed gently on ice on a shaker to mix for 10 min (total 30 min, kept on ice, vortex every 10 min). The samples were then centrifuged at ∼14,000*g* (13,380 rpm) for 15 min to pellet cell debris. The supernatant solution was separated after centrifugation.

The biotinylated proteins (cell lysate) were then incubated with streptavidin beads (125 μL) for 30 min at room temperature. Protein-coated beads were separated with a magnet for 3 min. The supernatant was removed, and the beads were washed with PBS containing 0.1% BSA. Further wash steps were done in the following sequence: wash with cold PBS (X2), 0.2% Triton ×100 (X1), and cold PBS (X3). After the last wash, the beads were resuspended in 50 μL of PBS. 20 μL of this suspension was mixed with 10 μL of laemmli SDS lysis buffer, vortexed, and heated for 15 min at 80−90 °C. Samples for chemoproteomics were run briefly for 5 min on the gel (to keep the proteins packed at the top of the gel), after which the gel was stained with Coomassie blue to enable accurate cutting of the protein containing region on the gel which was sent out for proteomic analysis at the UT Southwestern Proteomics core. Analysis by the Proteomics core was done using Proteome Discoverer 3.0 and was searched using the human protein database from UniProt.

In Gel Digestion. All washes are performed with slow vortexing. Wash each gel band 1−2× for 15 min with 500 μL 100 mM ammonium bicarbonate. After washing multiple times, the supernatant is removed and 10 mM TCEP is added to completely cover the gel band (approx 200 μL). Then, it is placed at 60 °C for 30 min. It is quickly spun and TCEP is removed with an aspirator or pipetteman. Gel bands 2−3× 15' are washed in 500 μL of 50:50 acetonitrile:100 mM ammonium bicarbonate. The supernatant was removed and 50 μL of acetonitrile was added to completely dry the gel band (should turn opaque). Acetonitrile was removed and speed vac for ∼5 min or until slices were completely dry. A 20 μg bottle of trypsin (Promega, sequence grade) was resuspended in 200 μL of trypsin resuspension buffer. Dilution of 1:10 with 25 mM ammonium bicarbonate (10 ng/μL final) was done; 200 ng of trypsin (20 μL) was added to dehydrated gel slices (or if sure of exact protein concentration, a 50:1 enzyme:substrate ratio can be used). The gel slices are incubated in trypsin for 10 min to rehydrate. Then, enough 25 mM ammonium bicarbonate was added to cover the gel bands and was placed at 37 °C overnight. The next morning, the supernatant was transferred into a clean tube and enough 5% formic acid was added to cover the gel bands and incubate at room temperature for 15 min. The supernatant was transferred to the tube with the supernatant from the o/n digestion. Enough acetonitrile was added to cover gel bands (approx 100−200 μL) and incubated at room temperature for 15 min. The supernatant was transferred to the tube with digested peptides. The acetonitrile elutions were repeated until gel bands had become completely opaque (2−3 times). Dry peptide sample to a final volume of <10 μL in speed vac was obtained. At this stage, peptides may be stored at −80° until analysis.

Samples for HMOX2 IP Western blot were allowed to run fully on the gel for 30 min and previously described immunoblotting protocol followed.

CETSA Protocol. Briefly, MDA-MB-468 cells were treated at 10 μM (**Au-Mac1**) for 2 h. After treatment, cells were trypsinized and washed with ice-cold PBS. After washing, the cell pellets were resuspended in ice-cold PBS containing 1× protease inhibitor cocktail and aliquoted in 100 μL volume into five tubes (corresponding to 5 different temperature treatments). The tubes were heated to 36, 40, 44, 48, and 52 °C for 3 min and immediately incubated at 25 °C for another 3 min. This was followed by three freeze−thaw cycles to fully lyse the cells. Cell lysates were next centrifuged at 20,000*g* for 20 min at 4 °C to remove the insoluble fractions. The supernatant was transferred into new prechilled Eppendorf tubes labeled appropriately, and the protein in the supernatant was denatured by adding Laemmli buffer-SDS Lysis buffer. This was boiled at 90 °C for 5−10 min, and this soluble content was used for Western blot detection.

Animals. Female, 5-week-old BALB/c mice were purchased from Charles River Laboratories (Wilmington, MA). All mice were quarantined for 1 week prior to use and kept in microisolator cages (four mice per cage) in a temperature- and humidity-controlled environment as per the Division of Laboratory Animal Research (DLAR) of the University of Kentucky. All mice were maintained in a pathogen-free environment under the care of DLAR of the University of Kentucky. Our study was performed in compliance with the NIH guidelines (NIH Publication No. 85−23 Rev. 1985) for the care and use of laboratory animals, and all experimental procedures were monitored and approved by the Institutional Animal Care and Use Committee (IACUC) of University of Kentucky (USA).

In Vivo Efficacy. Five female BALB/c mice (5 weeks) were received from Charles River Laboratories (Wilmington, MA), and they had an acclimation period of 1 week before being implanted with 1,000,000 4T1 cells subcutaneously on their flanks. Three days postimplantation, the mice were administered 10 mg/kg **Au-Mac1** intraperitoneally (IP), 0.2 mL/mouse formulated as 1% DMSO, 10%

https://doi.org/10.1021/acs.jmedchem.4c02952
J. Med. Chem. XXXX, XXX, XXX−XXX

Kolliphor, and 89% PBS. The control group was injected with a PBS solution containing 1% DMSO and 1% Kolliphor. Complex 1 injection, tumor-size/body-weighing measurements were performed 3 days a week, and mice were euthanized 19 days later (n = 2 for **Au-Mac1**, and n = 2 for vehicle control).

Hematoxylin and Eosin (H&E) Staining. The mice used in the in vivo experiment of **Au-Mac1** were sacrificed at day 14 after tumor cells(4T1) injection. Mice organs (heart, lung, liver, kidney, spleen, and tumor) were fixed in freshly prepared paraformaldehyde (4% in PBS), the fixation time was 24 h. And those processed for paraffin sectioning. The organs sections of 5 μm were stained with H&E staining and used for histological examination of the organs and tumor. A total of 5 sections per tissue (spanning the full depth of the organ) were examined and photographed using a Nikon Eclipse 55i microscope.

*Bio Distribution of **Au-Mac1**.* With four mice inoculated with 4T1 (1,000,000 cells), after 20 days, **Au-Mac1** was administered to mice by IP administration (0.2 mL, 10 mg/kg). Each tissue was obtained by sacrificing the mice (n = 2) after 19 days. Obtained tissues were boiled for 5 h at 60 °C with 70% nitric acid (0.5 mL) and then boiled again at 60 °C for 10 min by adding 35% hydrogen peroxide (0.5 mL). The solution turned yellow and was diluted as needed to measure the gold content using a Graphite Furnace Atomic Absorption Spectrometer (GF-AAS). Before measuring all samples, we measured the standard solution curves were measured. To accurately account for matrix effects, we prepared standard solutions in a matrix that closely resembles the sample matrix, that is, vehicle-treated mouse tissue (liver) spiked with known Au concentrations and analyzed by GFAAS.

■ ASSOCIATED CONTENT

Supporting Information

The Supporting Information is available free of charge at https://pubs.acs.org/doi/10.1021/acs.jmedchem.4c02952.

Crystal data and structure refinement for compounds **Au-Mac1**, **Au-Mac2**; ^{1}H, ^{13}C, ^{31}P spectra, HPLC traces, ESI-MS, and biotinylated Au-Mac1 probe synthesis. Dose response graphs for compounds **Au-Mac1−5**, Cell cycle, apoptosis, OCR for **Au-Mac1**, and standard curve for in vivo biodistribution of **Au-Mac1** (PDF)

Molecular formular strings (CSV)

Accession Codes

CCDC deposition numbers are 2233791 and 2233792.

■ AUTHOR INFORMATION

Corresponding Authors

Jill M. Kolesar − *Center for Pharmaceutical Research and Innovation, Department of Pharmaceutical Sciences, College of Pharmacy and Markey Cancer Center, University of Kentucky, Lexington, Kentucky 40536, United States*; Email: Jill.Kolesar@uky.edu

Samuel G. Awuah − *Department of Chemistry and Center for Bioelectronics and Nanomedicine, University of Kentucky, Lexington, Kentucky 40506, United States; Center for Pharmaceutical Research and Innovation, Department of Pharmaceutical Sciences, College of Pharmacy and Markey Cancer Center, University of Kentucky, Lexington, Kentucky 40536, United States*; orcid.org/0000-0003-4947-7283; Email: awuah@uky.edu

Authors

Sailajah Gukathasan − *Department of Chemistry, University of Kentucky, Lexington, Kentucky 40506, United States*

Chibuzor Olelewe − *Department of Chemistry, University of Kentucky, Lexington, Kentucky 40506, United States*

Libby Ratliff − *Department of Chemistry, University of Kentucky, Lexington, Kentucky 40506, United States*; orcid.org/0000-0002-0187-9921

Jong H. Kim − *Department of Chemistry, University of Kentucky, Lexington, Kentucky 40506, United States*

Alyson M. Ackerman − *Department of Chemistry, University of Kentucky, Lexington, Kentucky 40506, United States*; orcid.org/0000-0001-5609-0509

J. Robert McCorkle − *Center for Pharmaceutical Research and Innovation, Department of Pharmaceutical Sciences, College of Pharmacy, University of Kentucky, Lexington, Kentucky 40536, United States*

Sean Parkin − *Department of Chemistry, University of Kentucky, Lexington, Kentucky 40506, United States*

Gunnar F. Kwakye − *Department of Neuroscience, Oberlin College, Oberlin, Ohio 44074, United States*

Complete contact information is available at: https://pubs.acs.org/10.1021/acs.jmedchem.4c02952

Author Contributions

#S.G. and C.O. equally contributing authors.

Notes

The authors declare the following competing financial interest(s): S.G.A. has patents pending to University of Kentucky Research Foundation. S.G.A. serves on the advisory board and is Chief Executive Officer of Ayarissa Biosciences.

■ ACKNOWLEDGMENTS

We are grateful for financial support from the National Cancer Institute (NCI) R01CA258421-01 (S.G.A.) and the UK Igniting research collaboration support (J.K. and S.G.A.). The authors also acknowledge the support of the Center for Pharmaceutical Research and Innovation (NIH P20 GM130456). We would like to thank the following facilities at the University of Kentucky who provided support in the completion of the experiments detailed in this manuscript. The UK NMR Center is supported by NSF (CHE-997738) and the UK X-ray facility is supported by the MRI program from NSF (CHE-1625732). For the flow cytometry experiments, we would like to thank the UK Flow Cytometry and Immune Function Core supported by the Office of the Vice President of Research, the Markey Cancer Center, and the NCI Center Core Support Grant (P30 CA177558). TNBC cells were gifted by Dr. Kathleen O'Connor.

■ ABBREVIATIONS USED

ATP	adenosine triphosphate
AUC	area under the curve
DACH	diamino cyclohexane
DMEM	Dulbecco's modified eagle medium
ESI-MS	electrospray ionization mass spectrometry
FBS	fetal bovine serum
GF-AAS	graphite furnace atomic absorption spectrometry
HPLC	high performance liquid chromatogram
L-GSH	L-glutathione
MMP	mitochondria membrane potential
ORTEP	Oak Ridge thermal ellipsoid plot
PBS	phosphate buffer saline
PVDF	polyvinylidene difluoride
RIPA	radioimmunoprecipitation assay
TMRE	tetramethylrhodamine, ethyl ester
TNBC	triple negative breast cancer.

https://doi.org/10.1021/acs.jmedchem.4c02952
J. Med. Chem. XXXX, XXX, XXX−XXX

REFERENCES

(1) Mertens, R. T.; Gukathasan, S.; Arojojoye, A. S.; Olelewe, C.; Awuah, S. G. Next Generation Gold Drugs and Probes: Chemistry and Biomedical Applications. *Chem. Rev.* **2023**, *123*, 6612−6667.

(2) Shaw, C. F. Gold-Based Therapeutic Agents. *Chem. Rev.* **1999**, *99*, 2589−2600.

(3) Bartlett, N. Relativistic effects and the chemistry of gold. *Gold Bulletin* **1998**, *31*, 22−25.

(4) Schwerdtfeger, P.; Dolg, M.; Schwarz, W. H. E.; Bowmaker, G. A.; Boyd, P. D. W. Relativistic effects in gold chemistry. I. Diatomic gold compounds. *J. Chem. Phys.* **1989**, *91*, 1762−1774.

(5) Das, A.; Das, U.; Das, A. K. Relativistic effects on the chemical bonding properties of the heavier elements and their compounds. *Coord. Chem. Rev.* **2023**, *479*, No. 215000.

(6) Arojojoye, A. S.; Awuah, S. G. Functional utility of gold complexes with phosphorus donor ligands in biological systems. *Coord. Chem. Rev.* **2025**, *522*, No. 216208.

(7) Zou, T.; Lum, C. T.; Lok, C.-N.; Zhang, J.-J.; Che, C.-M. Chemical biology of anticancer gold(iii) and gold(i) complexes. *Chem. Soc. Rev.* **2015**, *44*, 8786−8801.

(8) Arojojoye, A. S.; Kim, J. H.; Olelewe, C.; Parkin, S.; Awuah, S. G. Chiral gold(III) complexes: speciation, in vitro, and in vivo anticancer profile. *Chem. Commun. (Camb)* **2022**, *58*, 10237−10240.

(9) Olelewe, C.; et al. Gold(III)-P-chirogenic complex induces mitochondrial dysfunction in triple-negative breast cancer. *iScience* **2022**, *25*, No. 104340.

(10) Kim, J. H.; Reeder, E.; Parkin, S.; Awuah, S. G. Gold(I/III)-Phosphine Complexes as Potent Antiproliferative Agents. *Sci. Rep* **2019**, *9*, 12335.

(11) Gukathasan, S.; Parkin, S.; Awuah, S. G. Cyclometalated Gold(III) Complexes Bearing DACH Ligands. *Inorg. Chem.* **2019**, *58*, 9326−9340.

(12) Gukathasan, S.; Awuah, S. G. Synthetic Strategies for the Preparation of Gold-based Anticancer Agents. in *Encyclopedia of Inorganic and Bioinorganic Chemistry*; Wiley, 1−32.

(13) Kim, J. H.; et al. Anticancer gold(iii)-bisphosphine complex alters the mitochondrial electron transport chain to induce in vivo tumor inhibition. *Chemical Science* **2021**, *12*, 7467−7479.

(14) Tong, K.-C.; et al. An anticancer gold(III)-activated porphyrin scaffold that covalently modifies protein cysteine thiols. *Proc. Natl. Acad. Sci. U. S. A.* **2020**, *117*, 1321−1329.

(15) Lu, Y.; et al. Recent development of gold(i) and gold(iii) complexes as therapeutic agents for cancer diseases. *Chem. Soc. Rev.* **2022**, *51*, 5518−5556.

(16) Skos, L.; et al. Gold-templated covalent targeting of the CysSec-dyad of thioredoxin reductase 1 in cancer cells. *Cell Rep. Phys. Sci.* **2024**, *5*, No. 102072.

(17) Schmidt, C.; Zollo, M.; Bonsignore, R.; Casini, A.; Hacker, S. M. Competitive profiling of ligandable cysteines in Staphylococcus aureus with an organogold compound. *Chem. Commun.* **2022**, *58*, 5526−5529.

(18) Muñoz-Sánchez, J.; Chánez-Cárdenas, M. E. A review on hemeoxygenase-2: focus on cellular protection and oxygen response. *Oxid. Med. Cell. Longev.* **2014**, *2014*, No. 604981.

(19) Chifman, J.; Laubenbacher, R.; Torti, S. A systems biology approach to iron metabolism. *Adv. Exp. Med. Biol.* **2014**, *844*, 201−225.

(20) Abbaspour, N.; Hurrell, R.; Kelishadi, R. Review on iron and its importance for human health. *J. Res. Med. Sci.* **2014**, *19*, 164−174.

(21) Torti, S. V.; Torti, F. M. Iron: The cancer connection. *Mol. Aspects Med.* **2020**, *75*, No. 100860.

(22) Consoli, V.; Sorrenti, V.; Grosso, S.; Vanella, L. Heme oxygenase-1 signaling and redox homeostasis in physiopathological conditions. *Biomolecules* **2021**, *11*, 589.

(23) Kinobe, R. T.; et al. Inhibition of the enzymatic activity of heme oxygenases by azole-based antifungal drugs. *J. Pharmacol. Exp. Ther.* **2006**, *319*, 277−284.

(24) Vlahakis, J. Z.; Vukomanovic, D.; Nakatsu, K.; Szarek, W. A. Selective inhibition of heme oxygenase-2 activity by analogs of 1-(4-chlorobenzyl)-2-(pyrrolidin-1-ylmethyl)-1H-benzimidazole (clemizole): exploration of the effects of substituents at the N-1 position. *Bioorg. Med. Chem.* **2013**, *21*, 6788−6795.

(25) Vukomanovic, D.; et al. Selective activation of heme oxygenase-2 by menadione. *Can. J. Physiol. Pharmacol.* **2011**, *89*, 861−864.

(26) Intagliata, S.; et al. Heme Oxygenase-2 (HO-2) as a therapeutic target: Activators and inhibitors. *Eur. J. Med. Chem.* **2019**, *183*, No. 111703.

(27) Kim, J.-J.; et al. A near-infrared probe tracks and treats lung tumor initiating cells by targeting HMOX2. *J. Am. Chem. Soc.* **2019**, *141*, 14673−14686.

(28) Eckstein, N. Platinum resistance in breast and ovarian cancer cell lines. *J. Exp. Clin. Cancer Res.* **2011**, *30*, 91.

(29) Siegel, R. L.; Miller, K. D.; Wagle, N. S.; Jemal, A. Cancer statistics, 2023. *Ca Cancer J. Clin* **2023**, *73*, 17−48.

(30) Li, Y.; Zhang, X.; Wang, Z.; Li, B.; Zhu, H. Modulation of redox homeostasis: A strategy to overcome cancer drug resistance. *Front. Pharmacol.* **2023**, *14*, No. 1156538.

(31) Tretter, V.; Hochreiter, B.; Zach, M. L.; Krenn, K.; Klein, K. U. Understanding cellular redox homeostasis: A challenge for precision medicine. *Int. J. Mol. Sci.* **2022**, *23*, 106.

(32) He, J. Z.; et al. Enhanced translation of heme oxygenase-2 preserves human endothelial cell viability during hypoxia. *J. Biol. Chem.* **2010**, *285*, 9452−9461.

(33) Yao, H.; Peterson, A. L.; Li, J.; Xu, H.; Dennery, P. A. Heme oxygenase 1 and 2 differentially regulate glucose metabolism and adipose tissue mitochondrial respiration: Implications for metabolic dysregulation. *Int. J. Mol. Sci.* **2020**, *21*, 7123.

(34) Hyun Kim, J.; Ofori, S.; Mertens, R. T.; Parkin, S.; Awuah, S. G. Water-Soluble Gold (III)−Metformin Complex Alters Mitochondrial Bioenergetics in Breast Cancer Cells. *ChemMedChem.* **2021**, *16*, 3222−3230.

(35) Huang, K.-B.; et al. Organometallic Gold(III) Complexes Similar to Tetrahydroisoquinoline Induce ER-Stress-Mediated Apoptosis and Pro-Death Autophagy in A549 Cancer Cells. *J. Med. Chem.* **2018**, *61*, 3478−3490.

(36) Sen, S.; et al. Rationally Designed Redox-Active Au(I) N-Heterocyclic Carbene: An Immunogenic Cell Death Inducer. *J. Am. Chem. Soc.* **2020**, *142*, 20536−20541.

(37) Olelewe, C.; Awuah, S. G. Mitochondria as a target of third row transition metal-based anticancer complexes. *Curr. Opin. Chem. Biol.* **2023**, *72*, No. 102235.

(38) Barros, M. H.; Nobrega, F. G.; Tzagoloff, A. Mitochondrial Ferredoxin Is Required for Heme A Synthesis inSaccharomyces cerevisiae. *J. Biol. Chem.* **2002**, *277*, 9997−10002.

(39) Foo, B. J.-A.; Eu, J. Q.; Hirpara, J. L.; Pervaiz, S. Interplay between mitochondrial metabolism and cellular redox state dictates cancer cell survival. *Oxid. Med. Cell. Longev.* **2021**, *2021*, No. 1341604.

(40) Molina, D. M.; et al. Monitoring drug target engagement in cells and tissues using the cellular thermal shift assay. *Science* **2013**, *341*, 84−87.

(41) Jafari, R.; et al. The cellular thermal shift assay for evaluating drug target interactions in cells. *Nat. Protoc.* **2014**, *9*, 2100−2122.

(42) Twig, G.; Shirihai, O. S. The Interplay Between Mitochondrial Dynamics and Mitophagy. *Antioxid. Redox Signal* **2011**, *14*, 1939−1951.

(43) Giacomello, M.; Pyakurel, A.; Glytsou, C.; Scorrano, L. The cell biology of mitochondrial membrane dynamics. *Nat. Rev. Mol. Cell Biol.* **2020**, *21*, 204−224.

(44) Herkenne, S.; Scorrano, L. OPA1, a new mitochondrial target in cancer therapy. *Aging (Albany N. Y.)* **2020**, *12*, 20931.

(45) Anderson, G. R.; et al. Dysregulation of mitochondrial dynamics proteins are a targetable feature of human tumors. *Nat. Commun.* **2018**, *9*, 1677.

https://doi.org/10.1021/acs.jmedchem.4c02952
J. Med. Chem. XXXX, XXX, XXX−XXX